Supporting information:

Experimental Section

Synthesis of TiO_2-HMSs: There are three steps for the synthesis of TiO_2 hollow microspheres assembly from nanosheets:

Step I is the synthesis of primary TiO_2-HMSs: Briefly, 15 ml of H_2O_2 (40 wt.%) was added to 65 ml of the mixed solution containing urea (2.42 g) and $(NH_4)_2TiF_6$ (1.19 g) under magnetic stirring. The resulting dark brown solution was transferred to a 100-ml Teflon-lined autoclave, which was then heated in an electric oven at 200°C for 10 h. After cooling it down to room temperature, the white precipitates were filtrated and washed with water for three times.

Step II is the transformation of primary TiO_2-HMSs into H_2TiO_3-HMSs: The precipitates obtained from step I were re-dispersed in 50 ml of NaOH solution (10 $mol \cdot L^{-1}$) under magnetic stirring, which was followed by hydrothermal reaction at 120°C for 3 h in a 100-ml Teflon-lined autoclave. The produced sodium titanate precipitates (Na_2TiO_3-HMSs) were collected and washed with water, which were then re-dispersed in 600 ml of HCl solution (0.1 $mol \cdot L^{-1}$) under magnetic stirring for 10 h to transform it into hydrogen titanate. The suspension was filtered and washed with water for several times. The obtained powder (H_2TiO_3-HMSs) was dried in an oven at 80°C for 6 h.

Step III is the fabrication of defective TiO_2-HMSs with Ov: The obtained H_2TiO_3-HMSs powder (2.0 g) was mixed with urea (6.0 g), and followed by calcination in a Muffle furnace at 550 °C for 4 h with a ramping rate of 5 $°C \cdot min^{-1}$.

For comparison, perfect TiO_2-HMSs (PT) was also prepared by direct calcination of 2.0 g of H_2TiO_3-HMSs powder under other identical conditions but in the absence of any urea.

Preparation of Au-SA/DT: Au-SA/DT was prepared based on a deposition–precipitation method. Briefly, 500 mg of DT powders were dispersed in 50 ml of water under magnetic stirring. 30 min later,

25 ml of $(NH_4)_2CO_3$ solution (1.0 M) and 25 ml of $HAuCl_4 \bullet 4H_2O$ solution (1.0 gL^{-1}) were dropwise added into the suspensions. After stirring for another 30 min, the mixed solution was aged at room temperature for 12 h, which was then filtrated and washed with water for 3 times. The resulted powders were heated in an oven at 70 ^oC for 12 h and followed by calcination at 250 °C for 4 h in argon gas.

The procedure for the synthesis of Au-NPs/PT is identical to that of Au-SA/DT but using PT as supporter instead of DT (see Table S1).

By adjusting the volume of $HAuCl_4$ solution, a series of single atomic Au modified defective TiO_2 samples were prepared under other identical conditions. For simplicity, these samples were denoted as Aux, where "x" represent the relative volume of $HAuCl_4$ solution (Table S2). The loading amounts of Au for these TiO_2 photocatalysts were determined by ICP-MS (SHIMADZU ICPMS-2030). From Table S2, it can be seen that the contents of Au in Au-SA/DT and Au-NPs/PT samples are 0.32 wt. % and 0.34 wt. %, respectively. Note that Au10 and Au-SA/DT are the same sample.

Characterization: Phase structure of the photocatalyst was determined on a D8-advance X-ray diffractometer. The morphology of the photocatalyst was observed on an S4800 field emission scanning electron microscope (FESEM) and a Tecnai G20 electron microscope (TEM). Nitrogen sorption-desorption isotherms were performed in a Micromeritics ASAP 2020 nitrogen adsorption apparatus. FT-IR spectrum was recorded on a NEXUIS-470 infrared spectrometer, and X-ray photoelectron spectroscopy (XPS) measurements were done in a Kratos XSAM800 XPS system. Powder UV-visible absorption spectrum was recorded on a UV-2550 spectrophotometer using $BaSO_4$ as a reflectance standard. The photoluminescence (PL) spectrum of the photocatalyst was recorded on a on an F-7000 Fluorescence Spectrophotometer (λ_{ex} = 330 nm). Transient PL decay spectrum was monitored at room temperature from FLSP-920 fluorescence spectrophotometer (λ_{ex} = 330 nm). Electron paramagnetic resonance (EPR) signal was obtained from JES-FA 200 EPR spectrometer, and electron spin-resonance (ESR) spectroscopy measurement was obtained in DMPO solution (methanol dispersion is used for DMPO-$\bullet O_2^-$ and aqueous dispersion is used for DMPO-•OH) under UV irradiation. High-angle-annular-

dark-field STEM (HADDF-STEM) image was obtained from a fifth order aberration-corrected transmission electron microscope (JEOL ARM200CF) with a dual-type EDS detector (JED-2300T), and X-ray absorption near-edge spectroscopy (XANES) measurements for the Au L_3-edge were performed in fluorescence mode on beamline 20-BM-B with electron energy of 7 GeV and an average current of 100 mA which is located in the Advanced Photon Source at Argonne National Laboratory. The radiation was monochromatized by a Si (111) double-crystal monochromator. XANES data reduction and analysis were processed by Athena software.

(Photo)electrochemical measurement: Photocurrent and electrochemical impedance spectroscopy (EIS) were measured on a three-electrode system in CHI760E electrochemical workstation. TiO_2 electrodes were prepared as follows: Firstly, 20 mg of the photocatalyst was dispersed in 1.0 ml of alcohol solution (volume ratio of ethanol and water was 1:1). After ultrasonicated for 30 min, 30 ul of naphthol was also added. The resulted slurry was then coated on an indium-tin oxide (ITO) glass electrode by a doctor-blade method. The ITO/TiO_2 electrode, Pt plate, and Ag/AgCl electrode were used as the working, counter, and reference electrodes, respectively. Na_2SO_4 solution (0.4 mol L^{-1}) was used as electrolyte solution. In photocurrent measurement, an LED lamp (3 W) emitted mainly at λ= 365±10 nm was used as the light source. EIS was measured under open circuit potential with the frequency of 0.1~1000 Hz.

In-situ DRIFTS analysis: In-situ DRIFTS were performed on a Tensor II FT-IR spectrometer (Bruker) equipped with a reaction chamber. Before adsorption and photocatalytic oxidation of acetone, the chamber was cleaned by purging with high purity He gas. Then, the mixed gases of acetone (100 ppm balanced in N_2 gas) and O_2 were introduced into the reaction chamber with a flow rate of 50 $mlmin^{-1}$ for each. An UV LED lamp is used as the light source to initiate photocatalytic oxidation of acetone over TiO_2-HMSs photocatalyst.

Density functional theory (DFT) calculations: All spin-polarized DFT-D2 calculation was conducted in "Vienna Ab-initio Simulation Package" (VASP code 5.4.1) through the generalized gradient

correlation function.[25] Cut-off energy and Gaussian trailing width were set to be 400eV and 0.2eV, respectively.[26] K point was 2×2×2. All structures and energy were converged to below 0.01eV. Heyd - Scuseria - Ernzerhof (HSE06) method was used to estimate the energy band structure and state density.[27,28] The super cell model as adopted to simulate TiO_2-HMSs with the exposure of 3×3×1 (0 0 1) crystal plane, and it was named PT; that containing oxygen vacancy TiO_2-HMSs was simulated by removing one oxygen atom in the super cell, and it was named DT; and the oxygen vacancy TiO_2 hollow microspheres deposited single atomic Au was imitated by one oxygen atom replaced one gold atom in the super cell, and named Au-SA/DT.

Adsorption energy (*E*ads) is defined as follows (eq. 1):

$$E_{ads} = E_{tot} - E_T - E_{mol} \quad (1)$$

Where, E_{tot}, E_T and E_{mol} denote the total energy of compounds, adsorbent (PT, DT or Au-SA/DT) and the adsorbed molecules after adsorption, respectively.

Photocatalytic oxidation of acetone: As acetone is a typical VOCs in industry, we chose it as a probe to evaluate the photocatalytic activity of TiO_2-HMSs. The setup for acetone oxidation is shown in Fig. S1. The volume of the reactor is 15 L and an UV lamp mainly emitted at 365 nm is used as the light source. Before photocatalytic reaction, 20 ml of aqueous solution containing 0.2 g of the TiO_2-HMSs photocatalyst was ultrasonicated for 10 min, which was then transferred to a glass watch and kept in an electric oven at 60 ^oC for evaporation. After cooling down to room temperature, the watch glass coated with a layer of TiO_2 film was moved into the reactor. Then, 10 μl of acetone was injected in the reactor. After establishment of the adsorption equilibrium (about 30 min), the UV lamp was turned on to initiate the photocatalytic oxidation of acetone. The concentrations of acetone and carbon dioxide in the reactor can be online detected through Photoacoustic IR Multigas Monitor (INNOVA Air Tech Instruments, Model 1412).

Table S1. Physical property of the photocatalyst.

Sample	supporter	S_{BET} (m^2g^{-1})	PV (cm^3g^{-1})	APS (nm)	<τ> (ns)
PT	Perfect TiO_2	77.8	0.43	22.1	1.13
DT	Defective TiO_2	88.9	0.46	20.5	2.34
Au-NP/PT	Perfect TiO_2	81.8	0.44	21.8	1.96
Au-SA/DT	Defective TiO_2	99.9	0.37	13.6	2.67

[a]Brunauer-Emmett-Teller (BET) surface area of the photocatalyst is determined by the multipoint BET method using the adsorption data in the relative pressure (P/P_0) range from 0.05 to 0.3.

[b]Pore volume (PV) is determined from the adsorption branch of the nitrogen isotherms at $P/P_0 = 0.994$.

[c]Average pore size (APS) is estimated from the adsorption branch of the nitrogen isotherms using the BJH method.

[d]The average lifetime of the transient photoluminescence.

Table S2. The contents of Au on different TiO_2 photocatalysts determined by ICP-MS.

Photocatalyst	supporter	volumes of solution (ml)		Au (wt.)%
		$(NH_4)_2CO_3$ (1.0 $molL^{-1}$)	$HAuCl_4 \bullet 4H_2O$ (1.0 gL^{-1})	
Au2	Defective TiO_2	5	5	0.06
Au5	Defective TiO_2	12.5	12.5	0.15
Au10 (Au-SA/DT)	Defective TiO_2	25	25	0.32
Au15	Defective TiO_2	37.5	37.5	0.47
Au20	Defective TiO_2	50	50	0.61
Au-NP/PT	Perfect TiO_2	25	25	0.34

Table S3. Comparing the relative photoreactivity of the photocatalyst towards acetone oxidation.

Sample	oxidized acetone (ppm)	Light source	References
P25	90	UV	[1]
TiO_2 nanosheets	160	UV	[1]
TiO_2 nanofibers	97	UV	[2]
TiO_2 nanosheets	102	UV	[3]
SnO_2/Zn_2SnO_4/graphene	27	UV	[4]
TiO_2 Hollow microspheres	35	UV	[5]
Au-SA/DT	214	UV	This work

Table S4. Assignment of the FTIR bands observed upon adsorption and the photocatalytic oxidation of acetone vapors on AS-Au/DT conditioned in He and O_2.

Wavenumber (cm^{-1})	Assignment	References
2974, 2930	acetone ν(C-H)	[6]
3008	mesityl oxide	[7]
1425, 1366	acetone $\nu_{as}(CH_3)$	[6]
1238	acetone ν(C-C)	[6]
3698	specific OH groups	[8]
3715	specific OH groups	[8]
3461	H_2O ν OH	[8]
2957	formate $\nu_{as}(COO) + \delta(CH)$	[6]
2870	aldehyde $\nu_s(CH)$	[6,8]
1720	acetaldehyde ν(C=O)	[9]
1444	acetate $\nu_s(COO)$	[8,9]
1745	formic acid	[9]
1354	formate $\nu_s(COO)$	[6,9]
1225	bicarbonates	[6,7,10]

Table S5. Reaction path of acetone over AS-Au/DT.

Serial number	Reaction equation	Reaction energy (eV)	Reaction type
(1)	$TiO_2 + hv \rightarrow h^+ + e^-$		excitation
(2)	$O_2 + e^- \rightarrow O_2^-$		formation of ROSs
(3)	$CH_3COCH_3 + * \rightarrow CH_3COCH_3*$	-0.27	acetone adsorption
(4)	$CH_3COCH_3* + O_2^- - e^- \rightarrow CH_3COO^- + CH_2O* + H^+$	-0.67	acetone decomposition
(5)	$CH_2O* + O_2^- - e^- \rightarrow HCOO^- + O* + H^+$	1.22	formic acid production
(6)	$HCOO^- + O* \rightarrow CO_2 + OH^- + *$	-3.01	formic acid decomposition
(7)	$CH_3COO* \rightarrow CO_2 + CH_3*$	1.04	acetic acid decomposition
(8)	$CH_3* + O_2^- \rightarrow CH_2O* + OH^-$	-0.86	formaldehyde formation
(9)	$CH_2O* + O_2^- - e^- \rightarrow HCOO^- + O* + H^+$	1.22	formic acid production
(10)	$HCOO^- + O* \rightarrow CO_2 + OH^- + *$	-3.01	formic acid decomposition
(11)	$H^+ + OH^- \rightarrow H_2O$		

Note: "*"represents the adsorption site in Au-SA/DT photocatalyst.

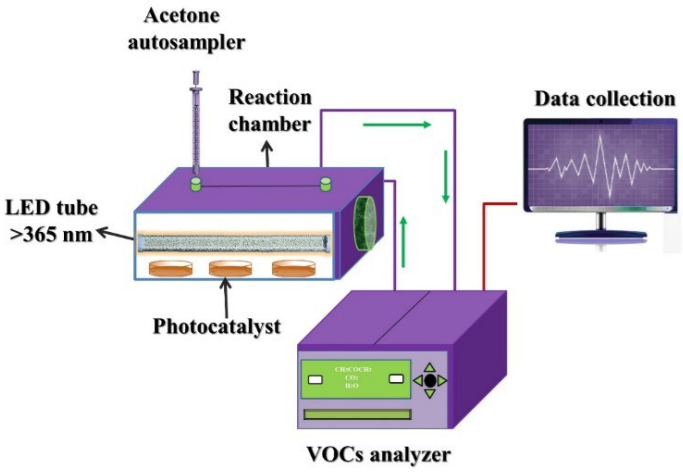

Fig. S1. Setup for photocatalytic acetone oxidation.

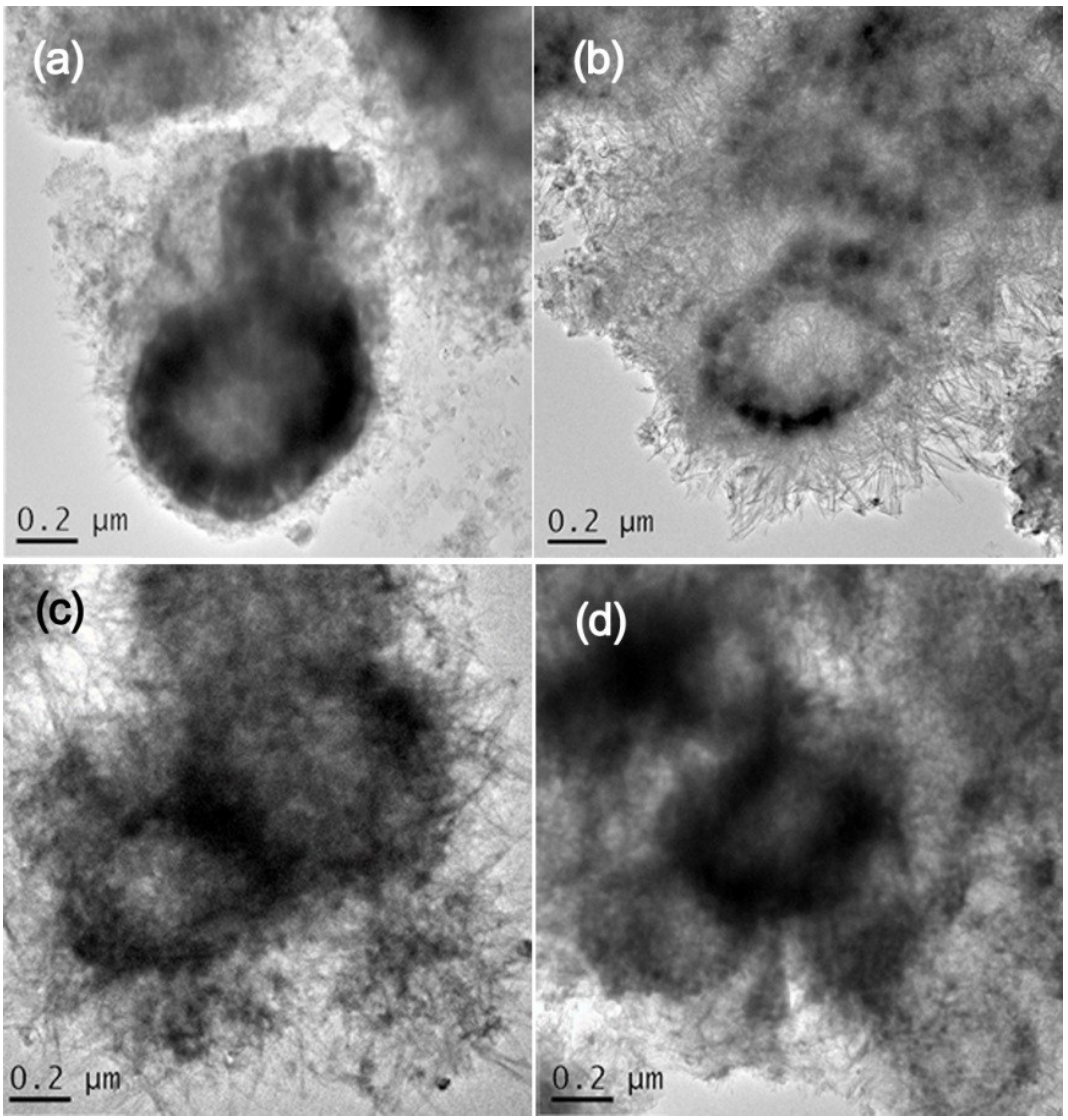

Fig. S2. TEM images of TiO_2-HMSs for PT (a), DT(b), Au-NP/PT (c) and Au-SA/DT (d) samples, respectively.

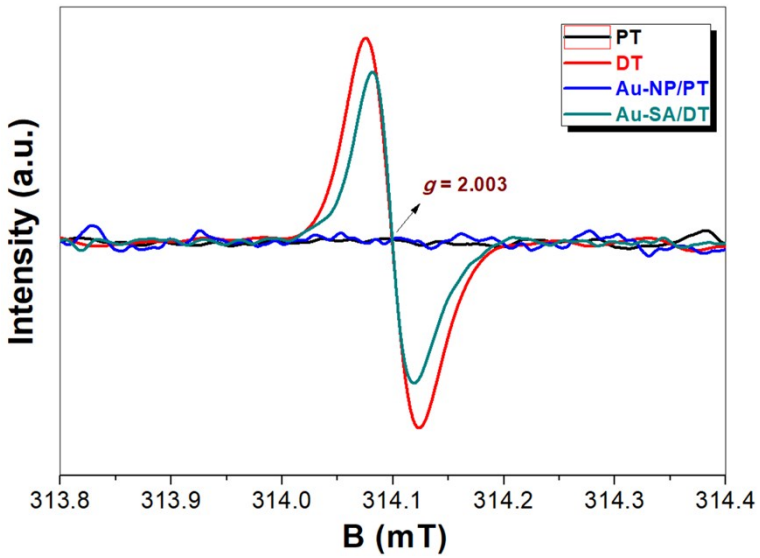

Fig. S3. EPR spectra of the TiO_2-HMSs photocatalysts.

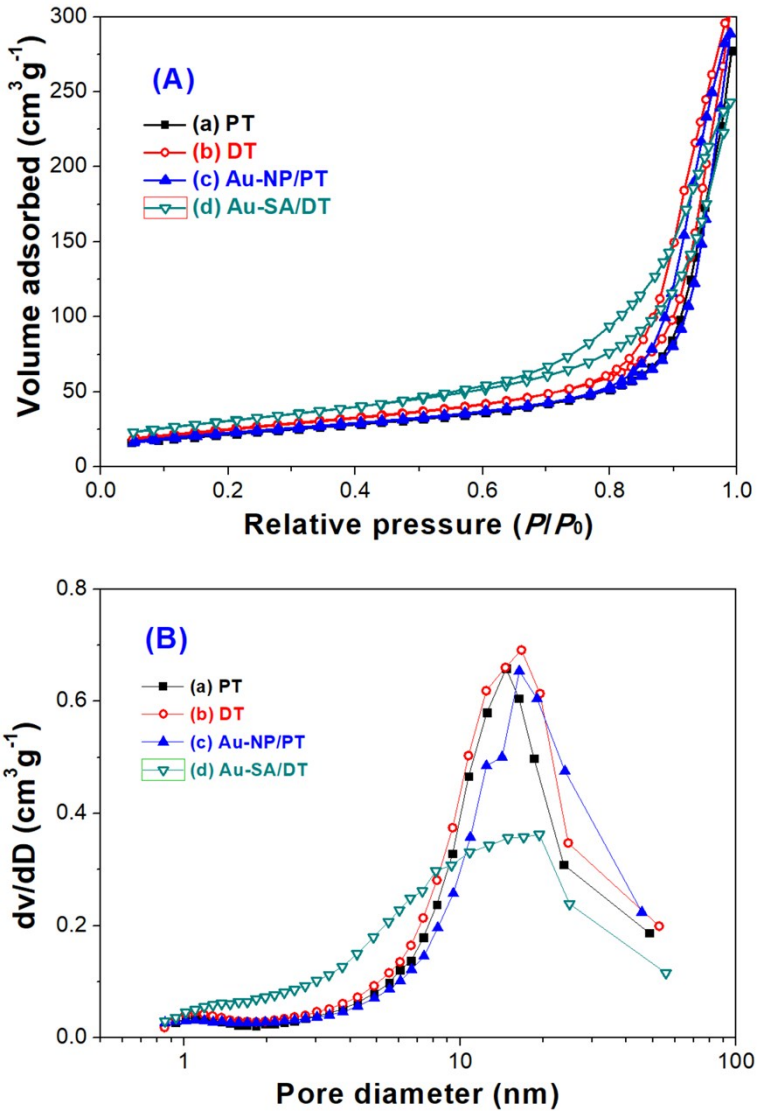

Fig. S4. Nitrogen sorption isotherms (A) and corresponding pore size distribution curves of TiO_2-HMSs photocatalysts.

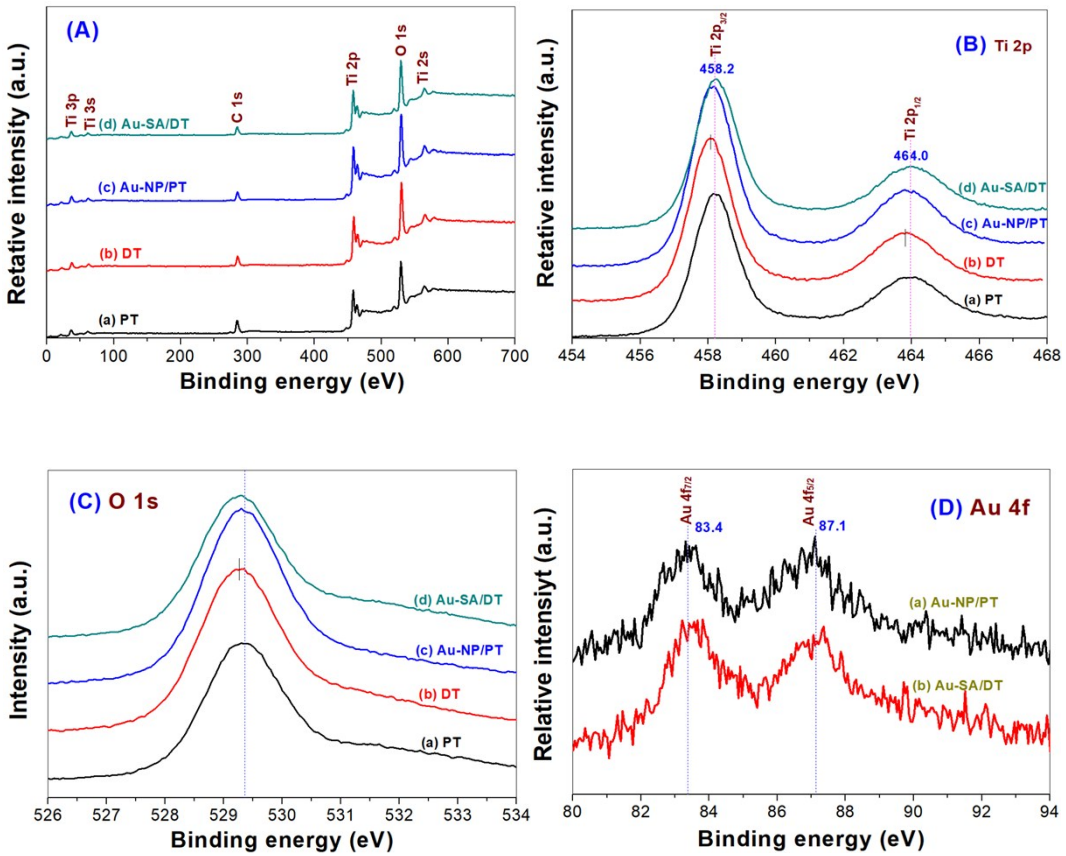

Fig. S5. XPS survey spectra (A) and corresponding high resolution XPS spectra in Ti 2p (B), O 1s (C) and Au 4f (D) regions of the TiO_2-HMSs photocatalysts.

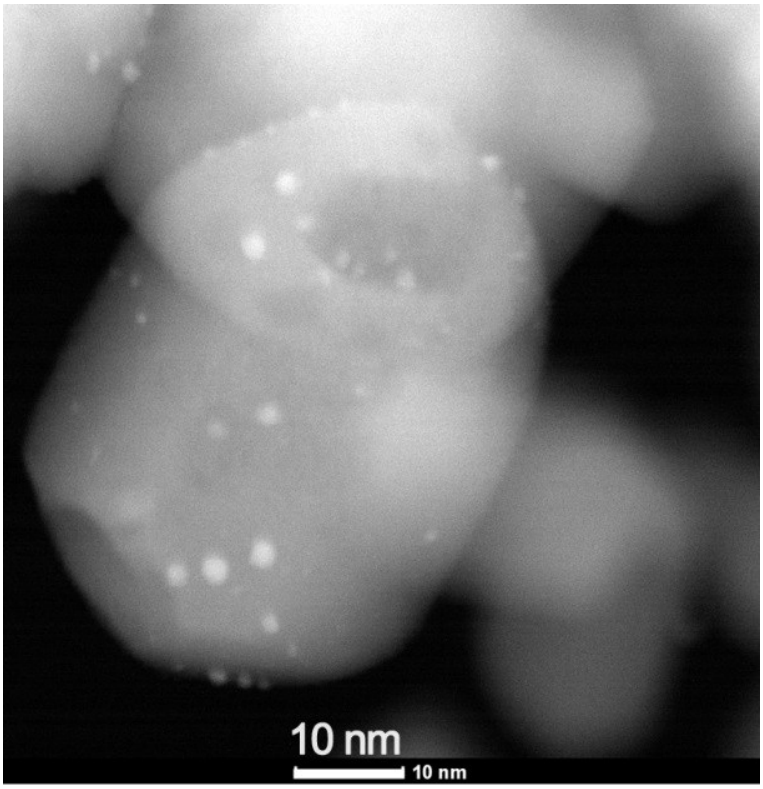

Fig. S6. HAADF-STEM image of Au-NP/PT sample.

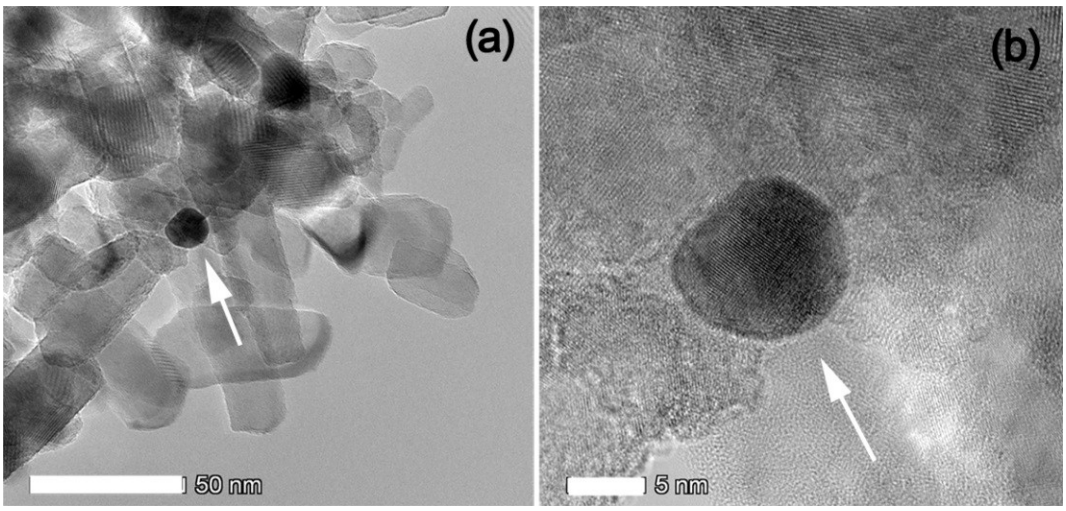

Fig. S7. TEM images of Au-NP/PT photocatalyst (arrows indicating the presence of Au nanoparticles).

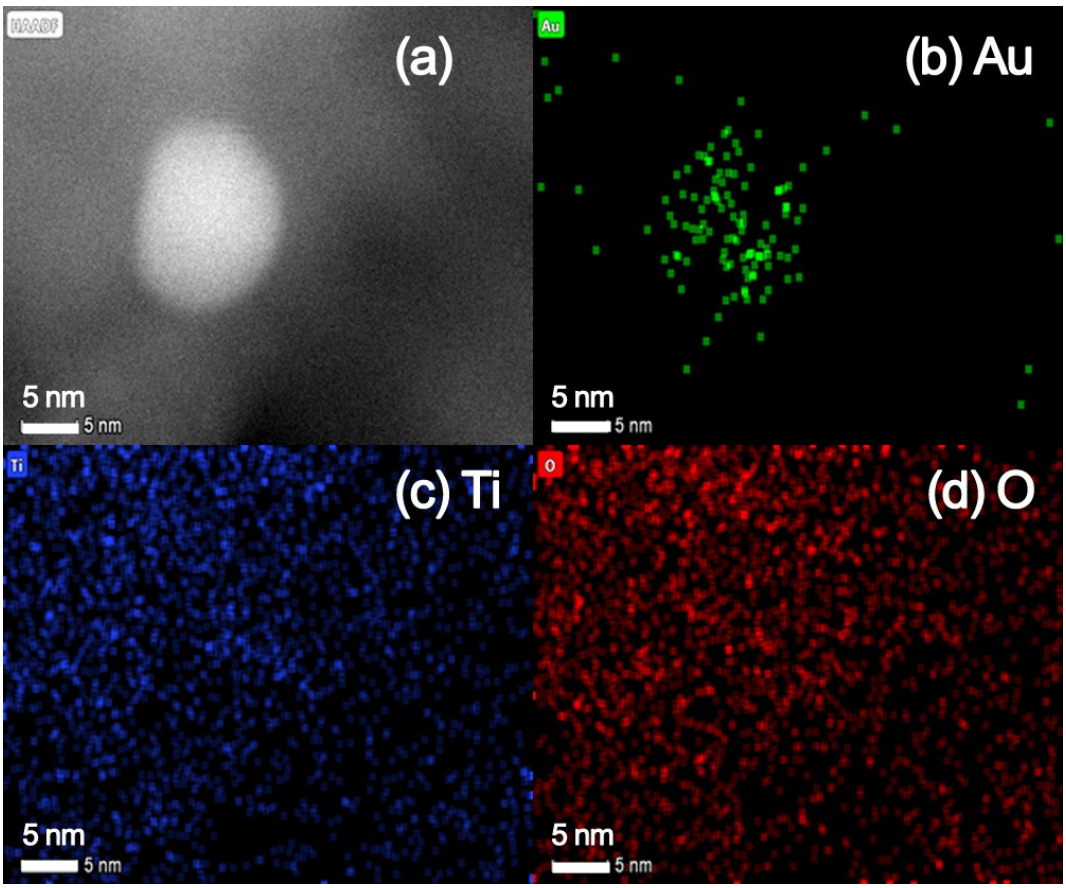

Fig. S8. HAADF-STEM image (a) and the corresponding element mappings for Au (b), Ti (c) and O (d) atoms of Au-NP/PT sample.

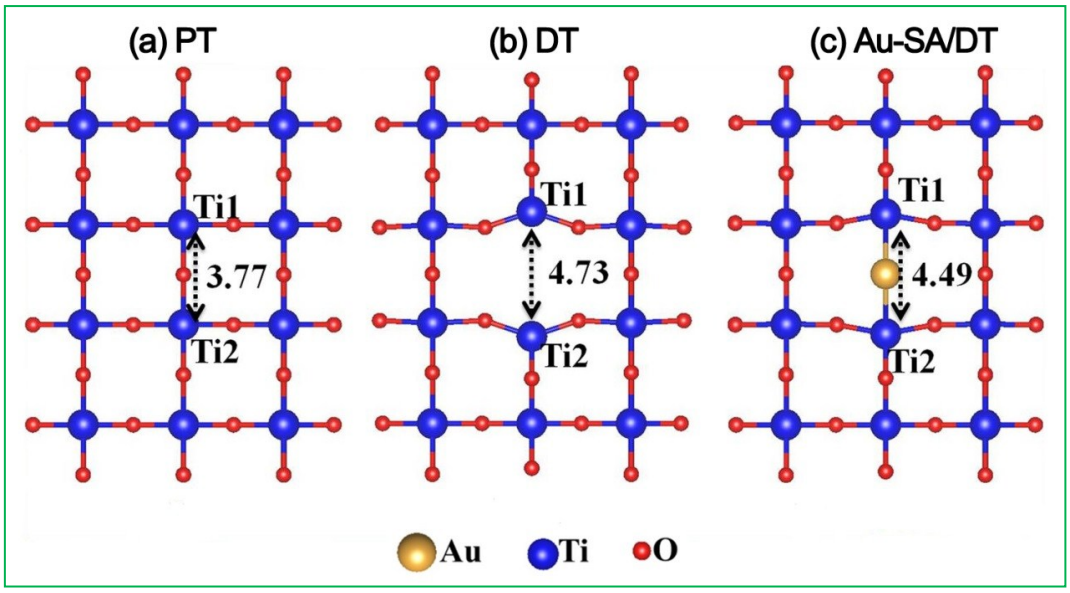

Fig. S9. The atomic model location of the optimized TiO_2 for perfect TiO_2 (a), defective TiO_2 (b) and SA-Au modified TiO_2 (c). The atomic distance unit: (Å).

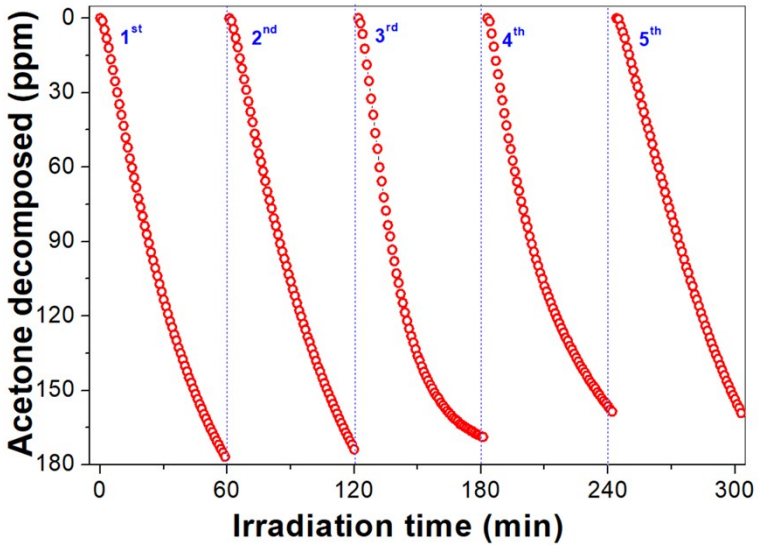

Fig. S10. Reusability of Au-SA/DT photocatalyst in photocatalytic oxidation of acetone.

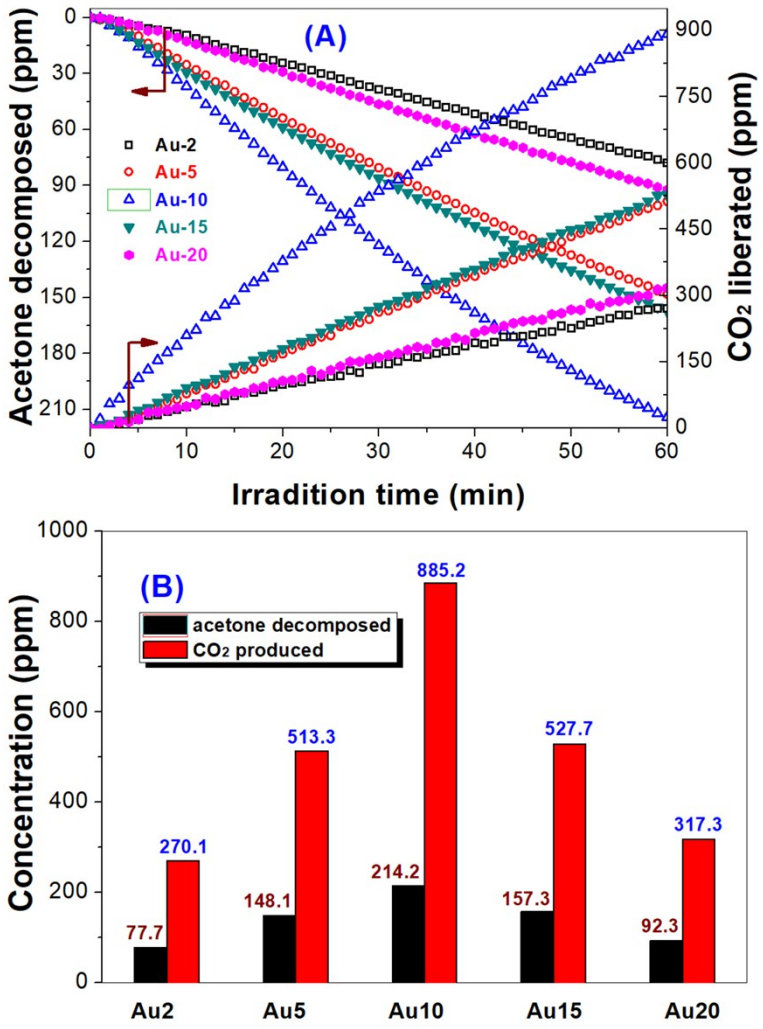

Fig. S11. Photocatalytic oxidation curves of acetone over Au-SA/TiO_2 with different Au loading amount (A) and the comparison of the photoreactivity (B).

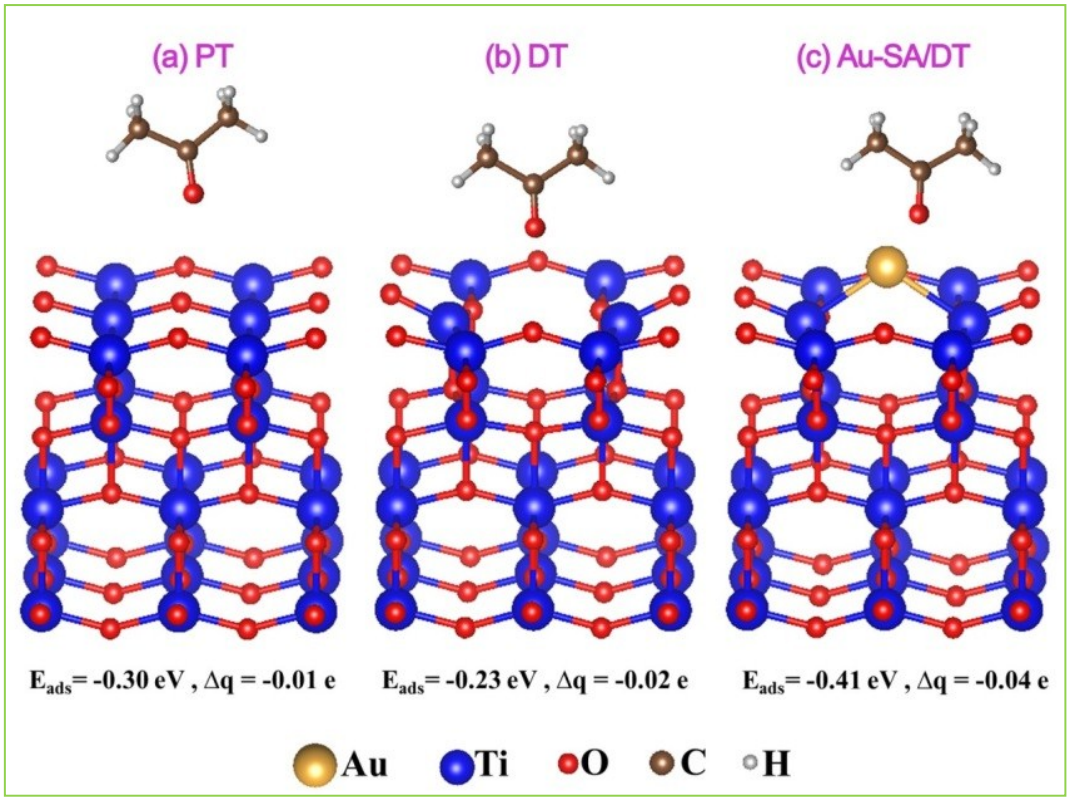

Fig. S12. Comparison of the optimized structural models for the adsorption of acetone over different photocatalysts: perfect TiO_2 (a), defective TiO_2 (b) and Au-SA-TiO_2 (c). E_{ads} the adsorption energy and Δq the Bader charge.

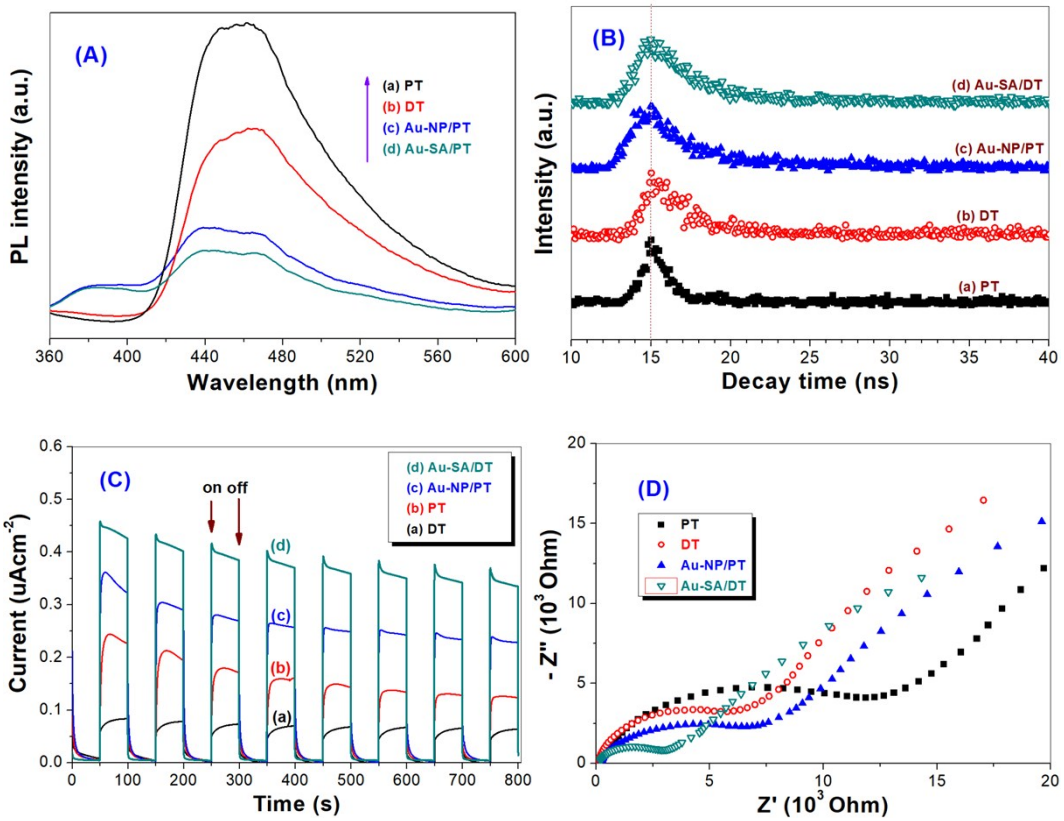

Fig. S13. Steady state photoluminescence spectra (A), transient photoluminescence (B), photocurrents (C) and EIS spectra (D) of TiO_2-HMSs photocatalysts, respectively.

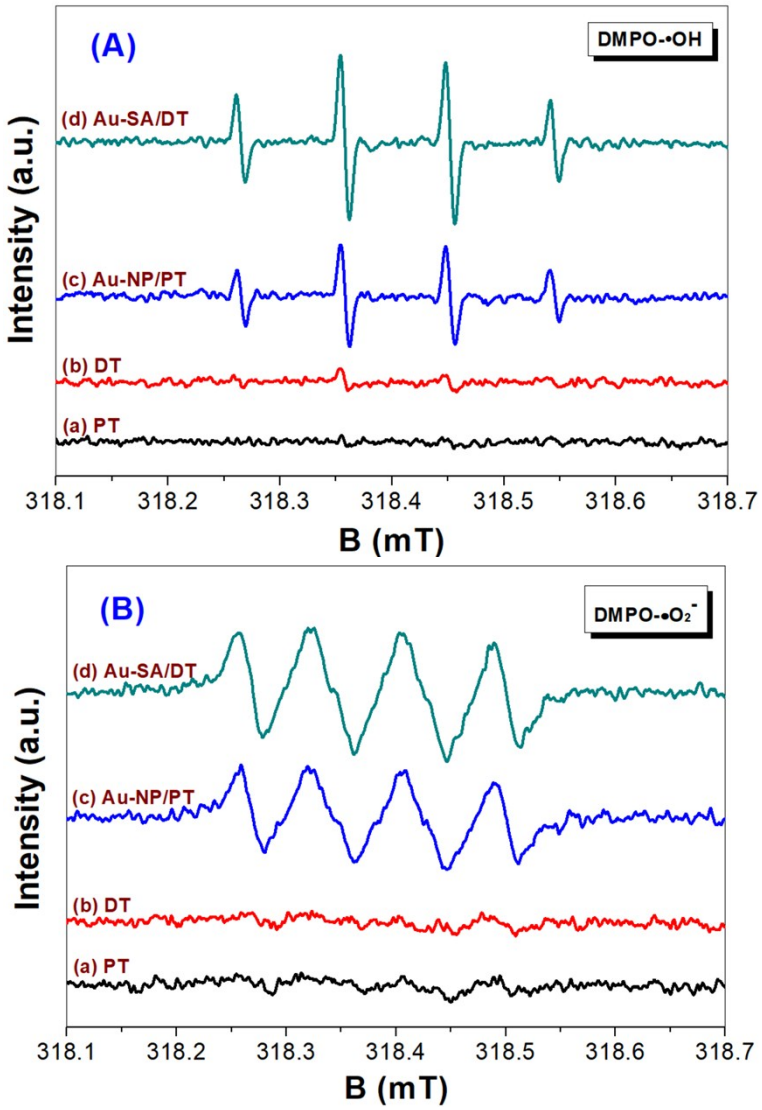

Fig. S14. Comparison of the ESR signals of DMPO-•OH (A) and DMPO-•O_2^- (B) adducts after illuminated TiO_2-HMSs photocatalysts (UV irradiation for 5 min.).

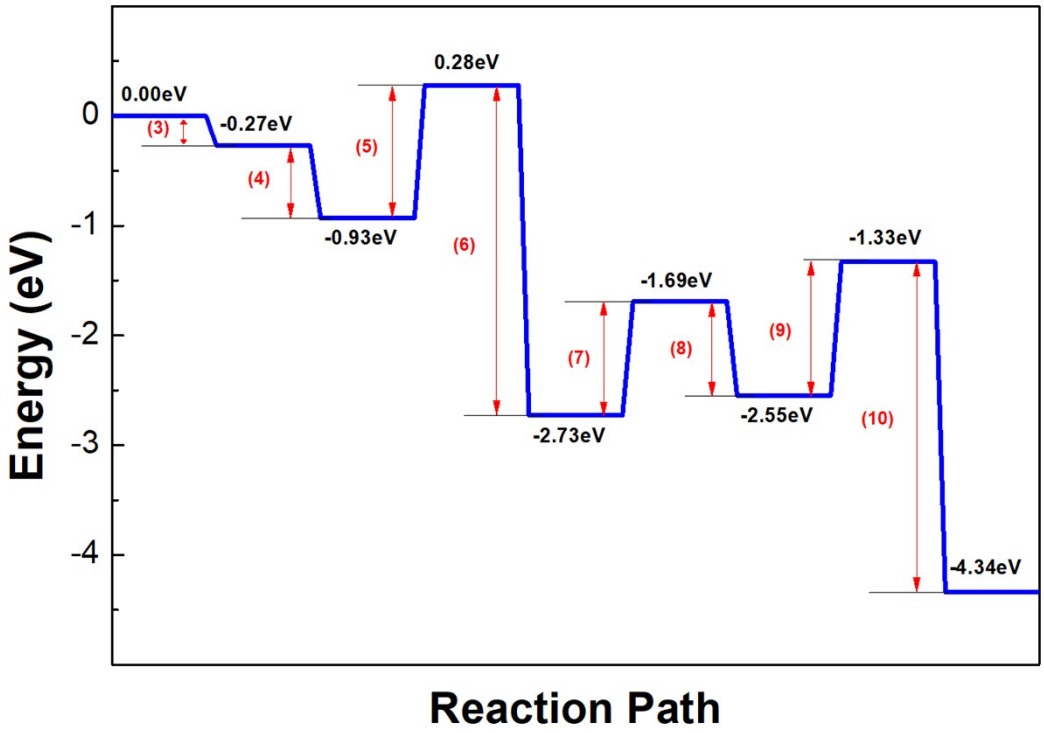

Fig. S15. Reaction path of Au-SA/DT photocatalytic oxidation of acetone.

Note: (1) The number of the reaction step can be seen from Table S3;

(2) Only the heat of reaction is considered here. When the reaction is exothermic, the reaction is considered to proceed smoothly; when the reaction absorbs heat, the energy barrier overcome by the reaction is equal to the heat of reaction.

.

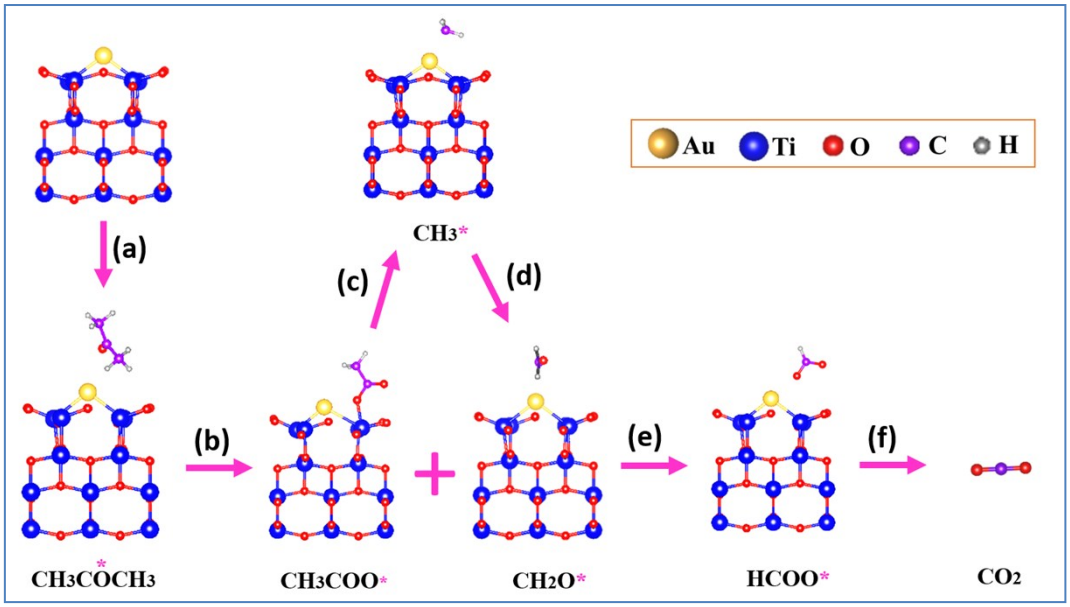

Fig. 16. Proposed photocatalytic degradation pathway of acetone over Au-SA/DT.

References:

[1] K.L. Lv, Q.J. Xiang, Jiaguo Yu, Effect of calcination temperature on morphology and photocatalytic activity of anatase TiO_2 nanosheets with exposed {001} facets. *Appl. Catal. B: Environ*. 2011, **104**, 275-281.

[2] Y.Y. Duan, L. Liang, K.L. Lv, Q. Li, M. Li, TiO_2 faceted nanocrystals on the nanofibers: Homojunction TiO_2 based Zscheme photocatalyst for air purification. *Appl. Surf. Sci*. 2018, **456**, 817-826.

[3] T. Shi, Y.Y. Duan, K.L. Lv, Z. Hu, Q. Li, M. Li, X.F. Li 1, Photocatalytic oxidation of acetone over high thermally stable TiO_2 nanosheets with exposed (001) facets, *Front. Chem*. 2018, **6**, 175.

[4] Yu.H. Li, X.F. Wu, Wi.K. Ho, K.L. Lv, Q. Li, M. Li, S.C. Lee, Graphene-induced surface vacancy of Zn_2SnO_4 for the enhanced visible-light-driven photocatalytic oxidation of NO and acetone, *Chem. Eng. J.* 2018, **336**, 200-210.

[5] L. Liang, K.N. Li, K.L. Lv, W.K. Ho, Y.Y. Duan, Highly photoreactive TiO_2 hollow microspheres with super thermal stability for acetone oxidation, *Chin. J. Catal.* 2017, **38**, 2085-2093.

[6] M. El-Maazawi, A.N. Finken, A.B. Nair, V.H. Grassian, Adsorption and photocatalytic oxidation of acetone on TiO_2: an in situ transmission FT-IR study. *J. Catal.* 2000, **191**, 138-146.

[7] J. Szanyi, J.H. Kwak, Photo-catalytic oxidation of acetone on a TiO_2 powder: An in situ FTIR investigation. *J. Mol. Catal. A: Chem.* 2015, **406**, 213-223.

[8] J.M. Coronado, S. Kataoka, I. Tejedor-Tejedor, M.A. Anderson, Dynamic phenomena during the photocatalytic oxidation of ethanol and acetone over nanocrystalline TiO_2: simultaneous FTIR analysis of gas and surface species. *J. Catal.* 2003, **219**, 219-230.

[9] E. Rekoske, M.A. Barteau, Competition between acetaldehyde and crotonaldehyde during adsorption and reaction on anatase and rutile titanium dioxide. *Langmuir.* 1999, **15**, 2061-2070.

[10] E.M. Kock, M. Kogler, T. Bielz, B. Klotzer, S. Penner, In situ FT-IR spectroscopic study of CO_2 and CO adsorption on Y_2O_3, ZrO_2, and yttria-stabilized ZrO_2. *J. Phys. Chem. C.* 2013, **117**, 17666-17673.